J. Astrophys. Astr. (0000) **000**: ####
DOI

arXiv:2010.01411v1 [astro-ph.SR] 3 Oct 2020

PAH and nbL Features Detection in Planetary Nebulae NGC 7027 and BD +30° 3639 with TIRCAM2 Instrument on 3.6m DOT

RAHUL KUMAR ANAND[1], SHANTANU RASTOGI[*1], BRIJESH KUMAR[2], ARPAN GHOSH[2], SAURABH SHARMA[2], D. K. OJHA[3] and S. K. GHOSH[3]

[1]Department of Physics, DDU Gorakhpur University, Gorakhpur 273009, India.
[2]Aryabhatta Research Institute of Observational Sciences, Manora Peak, Nainital-263001, India.
[3]Tata Institute of Fundamental Research, Homi Bhabha Road, Colaba, Mumbai 400 005, India.
[*]Corresponding author. E-mail: shantanu_r@hotmail.com

Abstract. High resolution infrared imaging observations of the young Planetary Nebulae NGC 7027 and BD +30° 3639, taken with the newly installed TIFR Infrared Camera-II (TIRCAM2) on 3.6m Devasthal Optical Telescope (DOT), ARIES, Nainital, are being reported. The images are acquired in J, H, K, polycyclic aromatic hydrocarbon (PAH) and narrow-band L (nbL) filters. The observations show emission from warm dust and PAHs in the circumstellar shells. The imaging of the two objects are among the first observations in PAH and nbL bands using TIRCAM2 on DOT. The NGC 7027 images in all bands show similar elliptical morphology with ∼6″.7 and ∼4″.5 semi-major and semi-minor axes. Considering size up to 10% of peak value the nebula extends upto 8″ from the central star revealing a multipolar evolution. The relatively cooler BD +30° 3639 shows a rectangular-ring shaped nebula. In J and H bands it shows an angular diameter of ∼8″, while a smaller ∼6″.9 size is observed in K, PAH and nbL bands. The 3.28 μm emission indicates presence of PAHs at about 6000 and 5000 AU from the central stars in NGC 7027 and BD +30° 3639 respectively. Analysis suggests domination of neutral PAHs in BD +30° 3639, while in NGC 7027 there is higher ionization and more processed PAH population.

Keywords. planetary nebulae, PAH, dust, outflows

1. Introduction

Planetary Nebulae (PNe) can be easily identified from other celestial objects for their strong emission lines in optical and infrared spectral regions. A star that has initial mass less than 8 $M_\odot$ ends its life through a period of extreme mass loss. As the star moves up the asymptotic giant branch (AGB), it undergoes severe mass-loss (10^{-7}–10^{-4} $M_\odot$ per year). The post-AGB or proto Planetary Nebulae phase is a short rapidly varying phase evolving towards the PNe phase (Van Winckel (2003); Kwok (2007) and references therein). During this phase the circumstellar dust shell moves away from the central star and temperature decreases from ∼400 to 100 K (Bedijn, 1987; Zijlstra et al., 1992). As the circumstellar shell moves away enough to expose the central hot core, the PNe is revealed. The central hot core ionizes the circumstellar shell exhibiting emission lines and continuum. Most PNe deviate from spherical symmetry and show spectacular bipolar or multipolar structures. The short transition period from post-AGB to evolved PNe is not well understood. This is an important evolutionary phase as the circumstellar shells also provide environments for formation of molecules and chemical evolution (Ziurys, 2006; Agúndez et al., 2008; Van de Sande et al., 2019). The post-AGB, proto-PNe with carbon rich circumstellar shells are also considered to be the breeding ground for polycyclic aromatic hydrocarbon (PAH) molecules (Frenklach and Feigelson, 1989; Cherchneff et al., 1992; Tielens, 2008) seen through their mid-infrared emission features.

Near- and mid-IR observations provide the high spatial and spectral resolution required to study and understand the form and content of PNe. The observed flux is a function of several factors viz. hydrogen bound-free continuum emission, recombination and collisionally excited lines, molecular hydrogen emission and continuum components from hot dust of the medium. There are also ionic emission lines (e.g. Ne, Ar, S, Mg etc.), broad silicate feature near 9.7 μm, and infrared emission band features. Many bright infrared nebulae show mid-IR emission features attributed to PAH molecules pumped by background UV radiations and are referred to as Aromatic Infrared Bands (AIBs) (Leger and Puget, 1984; Allamandola et al., 1985; Tielens, 2008; Rastogi et al., 2013). Several PNe have been observed from ground in the spectral range 8-13 μm (Russell et al., 1977; Aitken and Roche, 1982; Roche and Aitken, 1986), between 7.5 and 23 μm with IRAS low resolution spectrometer (Pot-

© Indian Academy of Sciences

tasch et al., 1986), Kuiper Airborne Observatory (Cohen et al., 1989), Infrared Space Observatory (3.6-160 μm) (Persi et al., 1999), and Stratospheric Observatory for Infrared Astronomy (SOFIA) (0.3-1600 μm) (Reinacher et al., 2018). All observations point towards the complex physical and chemical evolution in these objects.

There is correlation between the presence of molecular emission and the morphology of PNe, such that objects rich in molecular material are bipolar or butterfly nebulae (Hora et al., 1999; Kastner et al., 1996; Huggins et al., 1996; Huggins and Healy, 1989; Zuckerman and Gatley, 1988). High progenitor mass also correlates with this bipolar morphology type (Corradi and Schwarz, 1995). This suggests that the higher mass AGB progenitors that have high mass loss rates produce dense, long lived molecular envelopes (Hora et al., 1999). The carbon rich envelopes are considered primary source of interstellar PAHs (Latter, 1991), which seed the growth of amorphous carbon dust (Tielens, 2008). Yet, the PAH emission features are rarely observed in AGB stars, probably due to the effective low temperature of AGB photosphere which are unable to excite the PAH vibrational modes. The PAH features are observed in spectra of post-AGB and PNe where the circumstellar dust shell is heated by the hard UV radiation field from the hot core. Thus, indication of the location of photo-excited PAHs can be useful in the understanding of the molecular and morphological evolution.

The observations in near-IR and PAH emission are difficult from ground-based telescopes. The newly installed TIFR Near Infrared Imaging Camera-II (TIRCAM2), attached to the main axial port of 3.6 m Devasthal Optical Telescope (DOT), ARIES, Nainital (Baug et al., 2018; Kumar et al., 2018; Sagar et al., 2019), provides an unique opportunity to study the 3.28 μm PAH feature from ground. In the present communication the TIRCAM2 is used for near-IR, conventional as well as narrow wavebands, imaging studies of the two young and carbon rich planetary nebulae NGC 7027 and BD +30° 3639. NGC 7027 is in a rapid and key moment in its evolution when it is transiting from predominantly neutral molecular envelope to an ionized one (Kwok, 2000). BD +30° 3639 is a young planetary nebula that hosts Wolf-Rayet [WC] Central star and is round, highly symmetric low-excitation nebula (Balick, 1987). Both objects have significant AIB features (Peeters et al., 2002; van Diedenhoven et al., 2004). The observations in PAH band give insight into the location and environment where PAHs have abundance.

2. Observations and Data Reduction

2.1 *TIRCAM2 Imaging Observation*

The near-IR imaging of the two objects NGC 7027 and BD +30° 3639 are performed in J, H, K, PAH and nbL (narrow-band L) filters, with wavelengths centring at 1.20, 1.65, 2.19, 3.28 and 3.59 μm, respectively. Among the observed AIBs a significant feature attributed to aromatic C-H stretch vibrations falls around 3.28 μm, therefore the corresponding filter is called PAH filter. The TIRCAM2 is attached to the main axial port of Cassegrain focus (Figure 1) of the 3.6 m DOT (latitude 29°.1971 N, longitude 79°.6841 E, altitude: 2450 m) and provides sub-arcsecond spatial resolution. Both the targets are good sources for ground based observation due to their compactness and high surface brightness in the infrared (Werner et al., 2014). These are among the first observations in PAH band at 3.28 μm ($\triangle\lambda$ ~0.06 μm) using TIRCAM2 on DOT. The observations of NGC 7027 and BD +30° 3639 are recorded on the nights of 2017 October 13 and 2018 May 10 respectively.

The TIRCAM2 is a closed cycle Helium cooled near-IR imaging camera equipped with a larger Raytheon 512 x 512 pixels InSb Aladdin III Quadrant focal plane array (FPA). The operating temperature of detector is 35 K. The InSb array in TIRCAM2 is sensitive to photons in the 1-5 μm wavelength bands. However, the optics of TIRCAM2 restricts the operating wavelengths to below ~3.8 μm. The camera has been designed to accommodate seven selectable standard near-IR filters (Naik et al., 2012; Baug et al., 2018), which can be used for imaging observations. Field of view (FoV) of the TIRCAM2 on DOT is ~86″.5 x 86″.5 with a pixel scale of 0″.169 ± 0″.002. At Devasthal, the full width at half maxima (FWHM) of point source PSF (point spread function) during the observation nights was typically sub-arcsecond in all JHK bands.

During the observations standard strategy was adopted, which involves acquisition of dark frames and observations of flat frames with each filter during both morning and evening twilights. Between three-hundred to four-hundred different raw images were taken using JHK, PAH and nbL filters (Table 1). The source position was dithered to different positions on the array, ensuring that good pixels are present in all location of the image. On 2017 October 13 the K-band PSF was ~0″.76 and on 2018 May 10 it was ~0″.62. For NGC 7027, four frames of 20s exposure have been observed in J and H bands while in the K-band seven frames of 12s exposure were acquired to avoid detector saturation. In a similar way three frames of 8s exposure have been observed for BD +30° 3639 in J and H bands and

for the K band five frames of 5s exposure time were acquired.

Due to large background thermal emission in infrared, several hundred frames are taken in PAH and nbL bands with short exposure of 50ms for each frame in each dithered position for both the targets. Observation of nearby standard stars was also done, immediately before or after the observation of target source for photometric calibration. Dark frames were taken into account for the excess counts due to dark current in the detector. Flat-fielding is done using flat frames to remove non-uniformities in the science frames due to variation in pixel to pixel sensitivity and possible distortions caused by optics.

2.2 *Data Reduction*

The Image Reduction and Analysis Facility (IRAF) software[1] is used for photometric reduction. Standard procedure is followed, first each scientific frame was subtracted with corresponding exposure time master dark frame, which is median combine of all respective dark frames. Then the dark corrected frames were passed through flat fielding correction, i.e. divided by normalized master flat frame of the same filter to calibrate for any pixel to pixel sensitivity variation. The near-IR night sky brightness is influenced by OH emission lines, water vapour, zodiacal emission, thermal emission from the atmosphere and the telescope, and moonlight (Content, 1996; Sánchez et al., 2008). This make the near-IR sky few hundred times brighter than the sky in optical-bands and its removal from near-IR images of target source is one of the key steps in the data reduction process. In this work, the source position was dithered to different positions on the array, making it possible for the images of target itself to be used for sky subtraction. Since the observed target field was not crowded, therefore it was possible to construct master sky frame by median combining the science target frames for corresponding near-IR-band. Finally, the resultant same filter dithered science frames were aligned and added together, yielding a good signal to noise ratio image of the bright source.

The DAOPHOT-II (Stetson, 1992) package was used for photometric calibration of target sources. Both the PN objects are isolated in the science frames therefore aperture photometry is carried out in the J, H, K bands. The instrumental magnitude of the target sources was calibrated with respect to JHK standard sources (Hunt et al., 1998) available on the two nights. The offset value of magnitude of standard source in JHK band, has been directly used to calculate the magnitude of both the target PNe. The photometric results are listed in Table 2. For the photometry of NGC 7027 in K-band DAOPHOT-II gave error, probably because a large part of the K-band image overlaps bad patches in the lower side of the array. Measurements of various parameters viz. angular size of the objects, contour plots etc. are performed on SAO DS9 (Joye and Mandel, 2003), which is a powerful tool to visualize astronomical data and also for its analysis.

[1] http://iraf.net/

3. Results

3.1 *NGC 7027*

The final processed images in the five bands are shown in Figure 2. The nbL-band ($\lambda_{\rm cen}$ ~3.59 μm, $\triangle\lambda$ ~0.07 μm) falls close to the PAH-band ($\lambda_{\rm cen}$ ~3.28 μm, $\triangle\lambda$ ~0.06 μm), but will have no contribution of the emission due to the C-H stretch mode AIB. Therefore, the nbL observation may be considered a continuum feature in the PAH-band. A normalized continuum difference image, $(I_{PAH} - I_{nbL})/I_{nbL}$, highlighting the emission from the $AIB_{3.28}$ is shown in Figure 2(f). The central star of the NGC 7027 can be deciphered in the J and H bands while in the K band image it is too faint. It is also not visible in the PAH and nbL bands, implying that there is negligible near-IR emission from the central region. Two bright regions, seen in all the images along NE- and NW-direction, correspond to a surrounding torus of material (Meixner et al., 1993). These two bright regions have angular thickness ~1.″91 and ~2.″75 respectively and are symmetrically placed with respect to a NW - SE axis. The apparent mean angular diameter of NGC 7027 is measured as ~14″ (Table 3). The distance from the central star shows that major emissions from the nebula of NGC 7027 occur ~2.″51 away.

The images of NGC 7027 (Figure 2) demonstrate a nearly identical elliptical morphology with semi-major and semi-minor axes of ~6.″7 and ~4.″5, respectively. The major axis being inclined at an angle ~-30° from North, which is consistent with the morphology of the H II and photo-dissociation regions (Latter et al., 2000; Cox et al., 2002). In each band there are faint extended features that are more rectangular than elliptical. This deviation is better visualized in contour J, H, K images shown in Figure 3. Considering pixel values of upto 10% of the measured peak pixel value, the asymmetric features extend up to ~8″ from the central star in the ~-55° NW - SE direction. This is similar to the Paschen-α result of Lau et al. (2016).

The J band contour map, Figure 4, indicates outflows along the bi-directional arrows 1, 2, and 3. These correspond to the outflows identified by Cox et al. (2002) at ~-55°, ~4° and ~-28°. The PAH and nbL

features resemble elliptical morphology with a position angle along arrow 3 (∼-28°), while the extended features incline along arrow 1 (∼-55°).

3.2 *BD +30° 3639*

The images in the five bands and the PAH normalized continuum difference image of $AIB_{3.28}$ emission are shown in Figure 5. The bright central object and the surrounding relatively smooth nebula having similar morphology is seen in J, H and K filters. All the images have similar rectangular-ring shaped nebular emission feature and have two bright lobes in northern and southern parts. The northern lobe is slightly brighter than southern lobe in all observed bands (Hora et al., 1993). The deviation from spherical symmetry of the nebula is also suggested by the rectangular shapes in VLA observations (Bryce et al., 1997) and in spatial distribution of emission in radio continuum (Basart and Daub, 1987; Masson, 1989).

The angular diameter of the BD +30° 3639 is ∼8″ for J, H bands while the angular size in K, PAH and nbL bands is ∼6.″9 (see Table 4). The central object brightness extends up to ∼2″ in the J, H, K band images. The cavity immediately surrounding the central star, measured from the bright exterior of the central object to the inner edge of the shell, is ∼0.″6 along N-S and is ∼1″ along the E-W directions (Table 4).

As the central star is bright in J, H, K bands, the pixel count ratio of the central object to that of the surrounding nebula is obtained. The central object is nearly 4 times brighter in J and H while in the K band it is only ∼1.7 times brighter (Table 4). The angular thickness of the nebular ring is ∼1.″4.

The J, H, K contour images, shown in Figure 6, point to similar morphology but the position of the intense lobe towards south shifts slightly westward as the wavelength increases. This may be indicative of different matter distribution and outflow.

4. Discussion

The young planetary nebulae NGC 7027 and BD +30° 3639 are among the most studied and typical objects of their class. Both are in a similar stage of their evolution, with a carbon rich and molecular circumstellar medium. The first spectroscopic detection of the PAH related infrared emission bands was made on these PNe (Gillett et al., 1973). Both objects show similar 3.3 μm AIB feature, classified as class 'A' (van Diedenhoven et al., 2004). Despite these similarities the two objects are quite different in terms of their mass and temperature. While NGC 7027 is hot high excitation object, BD +30° 3639 is of relatively lower mass and low excitation. Some basic data for the two objects are compared in Table 5.

Both objects show cavity surrounding the central stars, where the high velocity winds from the hot core have pushed out the dust. As the winds from hot core move outward through the cavity, they are obstructed by torus of dust illuminating elliptical nebular shapes. The lower mass object BD +30° 3639 shows a smoother shape compared to NGC 7027, which being of higher mass has evolved faster with complex morphology indicative of multiple outflow episodes (Cox et al., 2002).

Contour images of the $AIB_{3.28}$ feature in the two objects are shown in Figures 7 and 8. For NGC 7027 the two bright lobes are clearly seen in the NE and SW, that fall somewhat along the ellipse minor-axis (Woodward et al., 1989). This is consistent with the extended asymmetric emission in longer wavelength AIBs (Lau et al., 2016). In BD +30° 3639 there are two bright regions in the northern part corresponding to the brighter JHK northern lobe. From the $AIB_{3.28}$ images average size of the PAH emission shell is obtained that defines the location of PAH molecules and also the region of possible PAH formation. The distance of this region from the central stars is about 6000 AU in NGC 7027 and about 5000 AU in BD +30° 3639 (Table 5).

The strength of the 3.3 μm AIB is much greater in NGC 7027 compared to that in BD +30° 3639 (van Diedenhoven et al., 2004). The circumstellar C/O ratio shows a linear correlation with the equivalent width of the feature (Smith and McLean, 2008), consistent with the higher C/O ratio in NGC 7027 (Table 5). It is well understood that the AIBs result from a mixture of neutral and ionized PAHs (Allamandola et al., 1999; Tielens, 2008; Rastogi et al., 2013). Laboratory and computational studies show that the 3.3 μm feature is prominent only in neutral PAHs and cations have negligible intensity in this band (Langhoff, 1996; Hudgins, 2002; Pathak and Rastogi, 2007; Maurya and Rastogi, 2015). Therefore, the similar 3.3 μm AIB feature in the two objects indicate a similar population of predominantly neutral PAHs. Indeed, for BD +30° 3639, a low-ionization fraction of PAHs is interpreted observationally (Bernard et al., 1994; Matsumoto et al., 2008), while an even distribution of PAH neutrals and cations is indicated for the hotter NGC 7027 (Maragkoudakis et al., 2020).

Though the 3.28 μm AIB in the two objects is of similar class 'A', the 6.2 μm AIB profile is altered. In NGC 7027 the 6.2 μm feature is classified as 'A' type, but in BD +30° 3639 it is of 'B' type (Peeters et al., 2002; van Diedenhoven et al., 2004). As the features vary with PAH size and charge states (Pathak and Rastogi, 2008; Maragkoudakis et al., 2020), this

difference in the 6.2 μm profile points towards variation in the PAH populations of the two objects. Generally PAH formation via bottom-up approach is envisaged in C-rich circumstellar shells of young PNe (Frenklach and Feigelson, 1989; Cherchneff et al., 1992; Cernicharo, 2004) and in high excitation regions PAHs may also form by top-down grain fragmentation. In BD +30° 3639 the C-rich stellar winds trigger PAH formation (Matsumoto et al., 2008), while in NGC 7027 rapid PAH formation is indicated from grain-grain collisions in the post-shock environment (Lau et al., 2016).

The route to formation of fresh PAHs in C-rich PNe (Frenklach and Feigelson, 1989; Cherchneff et al., 1992) indicates intermediate compounds as PAHs with side groups. In such PAHs e.g. with vinyl or phenyl substitution (Maurya and Rastogi, 2015; Singh and Rastogi, 2018) modes appear closer to 6.3 μm, that is similar to the class 'B' 6.2 μm AIB. These PAH derivatives could be part of the PAH population in BD +30° 3639. The PAH derivatives with aliphatic groups could also explain the step-like rise in continuum at around 3.6 μm by about 10% of the 3.28 μm peak (Ohsawa et al., 2016). The higher excitation and advanced evolution in NGC 7027 lead to a mixed PAH population including more processed and ionized PAHs.

5. Conclusion

The observations of diffused PAH emission are difficult and challenging from ground-based telescopes. The PNe images are successfully obtained in J, H, K, PAH and nbL bands. The present observations are among the first detections in PAH band (λ_{cen} ~3.28 μm, $\triangle\lambda$ ~0.06 μm) with the TIRCAM2 on DOT. The nbL band (λ_{cen} ~3.59 μm, $\triangle\lambda$ ~0.07 μm) images show continuum emission features of the surrounding PNe medium. The final frames showing the PNe in these bands were obtained by combining all dithered frames. The observations confirm the presence of emission due to aromatic C-H stretch vibrations at 3.28 μm and also throw light on the morphology of the objects and location of PAHs.

The JHK observations in NGC 7027 reveal elliptical morphology and features extending up to 8″ from the central star. BD +30° 3639 shows a rectangular-ring shaped nebula, with angular size of ~8″extending in J and H filters. A smaller extent of ~6″.9 is observed in K, PAH and nbL bands. The continuum normalized $AIB_{3.28}$ feature indicates that the location of PAHs is about 6000 AU and 5000 AU from the central star in NGC 7027 and BD +30° 3639 respectively. Analysis of the 6.2 μm AIB feature variations and its classification suggests a dominantly neutral and freshly formed PAH population in BD +30° 3639 while in NGC 7027 there is higher ionization and also possible PAH production by grain fragmentation.

Acknowledgements

This work is done under MoU between ARIES and DDU Gorakhpur University. RA acknowledges financial support from University Grants Commission, New Delhi under the Rajiv Gandhi National Fellowship scheme.

References

Agúndez M, Cernicharo J, Pardo JR, Fonfría Expósito JP, Guélin M, Tenenbaum ED, Ziurys LM, Apponi AJ (2008) Understanding the chemical complexity in Circumstellar Envelopes of C-Rich AGB stars: the case of IRC +10216. Astrophysics and Space Science 313(1-3):229–233, DOI 10.1007/s10509-007-9495-7, astro-ph/0702491

Aitken DK, Roche PF (1982) 8-13 μm spectrophotometry of compact planetary nebulae and emission line objects. Monthly Notices of the Royal Astronomical Society 200(2):217–237, DOI 10.1093/mnras/200.2.217, URL https://doi.org/10.1093/mnras/200.2.217, http://oup.prod.sis.lan/mnras/article-pdf/200/2/217/3539625/mnras200-0217.pdf

Akras S, Steffen W (2012) 'Distance mapping' and the 3D structure of BD +30° 3639. Monthly Notices of the Royal Astronomical Society 423(1):925–933, DOI 10.1111/j.1365-2966.2012.20928.x, URL https://doi.org/10.1111/j.1365-2966.2012.20928.x, https://academic.oup.com/mnras/article-pdf/423/1/925/18613038/mnras0423-0925.pdf

Allamandola LJ, Tielens AGGM, Barker JR (1985) Polycyclic aromatic hydrocarbons and the unidentified infrared emission bands: auto exhaust along the milky way. The Astrophysical Journal Letters 290:L25–L28, DOI 10.1086/184435

Allamandola LJ, Hudgins DM, Sandford SA (1999) Modeling the unidentified infrared emission with combinations of polycyclic aromatic hydrocarbons. The Astrophysical Journal 511(2):L115–L119, DOI 10.1086/311843, URL https://doi.org/10.1086%2F311843

Aller LH, Hyung S (1995) The nebular spectrum of BD +30° 3639, 0.36-1.05 μm. Monthly Notices of the Royal Astronomical Society 276(4):1101–1108, DOI 10.1093/mnras/276.4.1101

Balick B (1987) The Evolution of Planetary Nebulae. I. Structures, Ionizations, and Morphological Sequences. The Astrophysical Journal 94:671, DOI 10.1086/114504

Basart JP, Daub CT (1987) Temperature and Emission-Measure Distributions for Several Planetary Nebulae. The Astrophysical Journal 317:412, DOI 10.1086/165286

Baug T, Ojha DK, Ghosh SK, Sharma S, Pandey AK, Kumar B, Ghosh A, Ninan JP, Naik MB, D'Costa SLA, Poojary SS, Sand imani PR, Shah H, Krishna Reddy B, Pand ey SB, Chand H (2018) TIFR Near Infrared Imaging Camera-II on the 3.6 m Devasthal Optical Telescope. Journal of Astronomical Instrumentation 7(1):1850003-1881, DOI 10.1142/S2251171718500034, 1802.05008

Bedijn PJ (1987) Dust shells around Miras and OH/IR stars - Interpretation of IRAS and other infrared measurements. Astronomy & Astrophysics 186:136–152

Bernard JP, Giard M, Normand P, Tiphene D (1994) PAH distribution in BD 30+3639. Astronomy & Astrophysics 289:524–538

Bernard Salas J, Pottasch SR, Beintema DA, Wesselius PR (2000) The ISO-SWS Line Spectrum of Planetary Nebula NGC 7027. In: Salama A, Kessler MF, Leech K, Schulz B (eds) ISO Beyond the Peaks: The 2nd ISO Workshop on Analytical Spectroscopy, ESA Special Publication, vol 456, p 175

Bernard-Salas J, Pottasch SR, Wesselius PR, Feibelman WA (2003) Abundances of Planetary Nebulae ¡ASTROBJ¿BD+30 3639¡/ASTROBJ¿ and ¡ASTROBJ¿NGC 6543¡/ASTROBJ¿. Astronomy & Astrophysics 406:165–174, DOI 10.1051/0004-6361:20030777

Bryce M, Pedlar A, Muxlow T, Thomasson P, Mellema G (1997) New, sub-0.1-arcsec radio maps of two young planetary nebulae. Monthly Notices of the Royal Astronomical Society 284(4):815–820, DOI 10.1093/mnras/284.4.815

Cernicharo J (2004) The Polymerization of Acetylene, Hydrogen Cyanide, and Carbon Chains in the Neutral Layers of Carbon-rich Proto-planetary Nebulae. The Astrophysical Journal Letters 608(1):L41–L44, DOI 10.1086/422170

Cherchneff I, Barker JR, Tielens AGGM (1992) Polycyclic Aromatic Hydrocarbon Formation in Carbon-rich Stellar Envelopes. The Astrophysical Journal 401:269, DOI 10.1086/172059

Cohen M, Tielens AGGM, Bregman J, Witteborn FC, Rank DM, Allamandola LJ, Wooden D, Jourdain de Muizon M (1989) The infrared emission bands. III - Southern IRAS sources. The Astrophysical Journal 341:246–269, DOI 10.1086/167489

Content R (1996) Deep-Sky Infrared Imaging by Reduction of the Background Light. I. Sources of the Background and Potential Suppression of the OH Emission. The Astrophysical Journal 464:412, DOI 10.1086/177332

Corradi RLM, Schwarz HE (1995) Morphological populations of planetary nebulae: which progenitors? I. Comparative properties of bipolar nebulae. Astronomy & Astrophysics 293:871–888

Cox P, Huggins PJ, Maillard JP, Habart E, Morisset C, Bachiller R, Forveille T (2002) High resolution near-infrared spectro-imaging of NGC ~ 7027. Astronomy & Astrophysics 384(2):603–619, DOI 10.1051/0004-6361:20011780, URL https://doi.org/10.1051/0004-6361:20011780

van Diedenhoven B, Peeters E, Kerckhoven CV, Hony S, Hudgins DM, Allamandola LJ, Tielens AGGM (2004) The profiles of the 3–12 micron polycyclic aromatic hydrocarbon features. The Astrophysical Journal 611(2):928–939, DOI 10.1086/422404, URL https://doi.org/10.1086%2F422404

Frenklach M, Feigelson ED (1989) Formation of Polycyclic Aromatic Hydrocarbons in Circumstellar Envelopes. The Astrophysical Journal 341:372, DOI 10.1086/167501

Gillett FC, Forrest WJ, Merrill KM (1973) 8 - 13-micron spectra of NGC 7027, BD +30 3639, and NGC 6572. The Astrophysical Journal 183:87, DOI 10.1086/152211

Hora JL, Deutsch LK, Hoffmann WF, Fazio GG, Shivanandan K (1993) Near- and Mid-Infrared Imaging of the Planetary Nebulae BD +30 degrees 3639 and IC 418. The Astrophysical Journal 413:304, DOI 10.1086/172998

Hora JL, Latter WB, Deutsch LK (1999) Investigating the Near-Infrared Properties of Planetary Nebulae. II. Medium-Resolution Spectra. The Astrophysical Journal Supplement Series 124(1):195–240, DOI 10.1086/313256, URL https://doi.org/10.1086%2F313256

Hudgins DM (2002) Interstellar polycyclic aromatic compounds and astrophysics. Polycyclic Aromatic Compounds 22(3-4):469–488, DOI 10.1080/10406630290103852,

URL https://www.tandfonline.com/doi/abs/10.1080/10406630290103852, https://www.tandfonline.com/doi/pdf/10.1080/10406630290103852

Huggins PJ, Healy AP (1989) CO in planetary nebulae. The Astrophysical Journal 346:201–211, DOI 10.1086/168001

Huggins PJ, Bachiller R, Cox P, Forveille T (1996) The molecular envelopes of planetary nebulae. Astronomy & Astrophysics 315:284–302

Hunt LK, Mannucci F, Testi L, Migliorini S, Stanga RM, Baffa C, Lisi F, Vanzi L (1998) Northern JHK Standard Stars for Array Detectors. The Astronomical Journal 115(6):2594–2603, DOI 10.1086/300349, URL https://doi.org/10.1086%2F300349

Joye WA, Mandel E (2003) New Features of SAOImage DS9, Astronomical Society of the Pacific Conference Series, vol 295, p 489

Kastner JH, Weintraub DA, Gatley I, Merrill KM, Probst RG (1996) H_2 Emission from Planetary Nebulae: Signpost of Bipolar Structure. The Astrophysical Journal 462:777, DOI 10.1086/177192

Kumar B, Omar A, Maheswar G, Pand ey AK, Sagar R, Uddin W, Sanwal BB, Bangia T, Kumar TS, Yadav S, Sahu S, Pant J, Reddy BK, Gupta AC, Chand H, Pandey JC, Joshi MK, Jaiswar M, Nanjappa N, Purushottam, Yadav RKS, Sharma S, Pand ey SB, Joshi S, Joshi YC, Lata S, Mehdi BJ, Misra K, Singh M (2018) 3.6-m Devasthal Optical Telescope Project: Completion and first results. Bulletin de la Societe Royale des Sciences de Liege 87:29–41

Kwok S (2000) The Origin and Evolution of Planetary Nebulae. Cambridge Astrophysics, Cambridge University Press, DOI 10.1017/CBO9780511529504

Kwok S (2007) Planetary nebulae. Scholarpedia 2(9):4338, DOI 10.4249/scholarpedia.4338, revision #138051

Langhoff SR (1996) Theoretical infrared spectra for polycyclic aromatic hydrocarbon neutrals, cations, and anions. The Journal of Physical Chemistry 100(8):2819–2841, DOI 10.1021/jp952074g, URL https://doi.org/10.1021/jp952074g, https://doi.org/10.1021/jp952074g

Latter WB (1991) Large molecule production by mass-losing carbon stars - The primary source of interstellar polycyclic aromatic hydrocarbons? The Astrophysical Journal 377:187–191, DOI 10.1086/170346

Latter WB, Dayal A, Bieging JH, Meakin C, Hora JL, Kelly DM, Tielens AGGM (2000) Revealing the Photodissociation Region:HST/NICMOS Imaging of NGC 7027. The Astrophysical Journal 539(2):783–797, DOI 10.1086/309252, URL https://doi.org/10.1086%2F309252

Lau RM, Werner M, Sahai R, Ressler ME (2016) Evidence from sofia imaging of polycyclic aromatic hydrocarbon formation along a recent outflow in ngc 7027. The Astrophysical Journal 833(1):115, DOI 10.3847/1538-4357/833/1/115, URL https://doi.org/10.3847%2F1538-4357%2F833%2F1%2F115

Leger A, Puget JL (1984) Identification of the 'unidentified' IR emission features of interstellar dust? Astronomy & Astrophysics 137:L5–L8

Leuenhagen U, Hamann WR, Jeffery CS (1996) Spectral analyses of late-type WC central stars of planetary nebulae. Astronomy & Astrophysics 312:167–185

Li J, Harrington JP, Borkowski KJ (2002) The Angular Expansion and Distance of the Planetary Nebula BD +30°3639. The Astrophysical Journal 123(5):2676–2688, DOI 10.1086/340078, astro-ph/0202170

Maragkoudakis A, Peeters E, Ricca A (2020) Probing the size and charge of polycyclic aromatic hydrocarbons. Monthly Notices of the Royal Astronomical Society 494(1):642–664, DOI 10.1093/mnras/staa681, URL https://doi.org/10.1093/mnras/staa681, https://academic.oup.com/mnras/article-pdf/494/1/642/32993215/staa681.pdf

Masson CR (1989) The structure of NGC 7027 and a determination of its distance by measurement of proper motions. The Astrophysical Journal 336:294–303, DOI 10.1086/167011

Matsumoto H, Sakon I, Onaka T, Sako S, Miyata T, Kataza H, Okada Y, Okamoto YK, Honda M, Yamashita T, Takahashi H, Fujiyoshi T (2008) Mid-Infrared Observations of Planetary Nebula BD +30 3639: Evolution and Distribution of Unidentified IR Band Carriers. The Astrophysical Journal 677(2):1120–1131, DOI 10.1086/533526

Maurya A, Rastogi S (2015) Vibrational spectroscopic study of vinyl substituted polycyclic aromatic hydrocarbons. Spectrochimica Acta Part A: Molecular and Biomolecular Spectroscopy 151:1 – 10, DOI https://doi.org/10.1016/j.saa.2015.06.069, URL http://www.sciencedirect.com/science/article/pii/S1386142515300093

Meixner M, Skinner CJ, Temi P, Rank D, Bregman J, Ball JR, Keto E, Arens JF, Jernigan JG (1993) 2–12.5 Micron Imaging of IRAS 21282+5050: The Structure of a Young Planetary Nebula. The Astrophysical Journal 411:266, DOI 10.1086/172826

Mellema G (2004) On expansion parallax distances for planetary nebulae. Astronomy & Astrophysics 416:623–629, DOI 10.1051/0004-6361:20034485, astro-ph/0312140

Naik M, Ojha D, Ghosh S, Poojary S, Jadhav R, Meshram G, Sandimani P, Bhagat S, D'Costa S, Gharat S, Bakalkar C, Ninan JP, Joshi J (2012) Tircam2: The tifr near infrared imaging camera. Bulletin of the Astronomical Society of India 40

Ohsawa R, Onaka T, Sakon I, Matsuura M, Kaneda H (2016) AKARI/IRC Near-infrared Spectral Atlas of Galactic Planetary Nebulae. The Astrophysical Journal 151(4):93, DOI 10.3847/0004-6256/151/4/93, 1604.00884

Pathak A, Rastogi S (2007) Theoretical spectra of PAHs in modeling astrophysical IR features. Advances in Space Research 40(11):1620–1627, DOI 10.1016/j.asr.2007.08.011

Pathak A, Rastogi S (2008) Modeling the interstellar aromatic infrared bands with co-added spectra of PAHs. Astronomy & Astrophysics 485(3):735–742, DOI 10.1051/0004-6361:20066618, 0804.2555

Peeters E, Hony S, Van Kerckhoven C, Tielens AGGM, Allamandola LJ, Hudgins DM, Bauschlicher CW (2002) The rich 6 to 9 μm spectrum of interstellar PAHs. Astronomy & Astrophysics 390:1089–1113, DOI 10.1051/0004-6361:20020773, astro-ph/0205400

Persi P, Cesarsky D, Marenzi AR, Preite-Martinez A, Rouan D, Siebenmorgen R, Lacombe F, Tiphene D (1999) Mid-infrared spectral images of planetary nebulae with ISOCAM. Astronomy & Astrophysics 351:201–211

Pottasch SR, Preite-Martinez A, Olnon FM, Mo JE, Kingma S (1986) IRAS spectra planetary nebulae. III. Astronomy & Astrophysics 161:363–375

Rastogi S, Pathak A, Maurya A (2013) Polycyclic aromatic hydrocarbon molecules in astrophysics. AIP Conference Proceedings 1543(1):49–63, DOI 10.1063/1.4812599, URL https://aip.scitation.org/doi/abs/10.1063/1.4812599, https://aip.scitation.org/doi/pdf/10.1063/1.4812599

Reinacher A, Graf F, Greiner B, Jakob H, Lammen Y, Peter S, Wiedemann M, Zeile O, Kaercher HJ (2018) The SOFIA Telescope in Full Operation. Journal of Astronomical Instrumentation 7(4):1840007, DOI 10.1142/S225117171840007X

Roche PF, Aitken DK (1986) The infrared spectral properties of planetary nebulae. Monthly Notices of the Royal Astronomical Society 221(1):63–76, DOI 10.1093/mnras/221.1.63, URL https://doi.org/10.1093/mnras/221.1.63, http://oup.prod.sis.lan/mnras/article-pdf/221/1/63/18522000/mnras221-0063.pdf

Russell RW, Soifer BT, Merrill KM (1977) Observations of the unidentified 3.3 micron emission feature in nebulae. The Astrophysical Journal 213:66–70, DOI 10.1086/155129

Sagar R, Kumar B, Omar A (2019) The 3.6 meter Devasthal Optical Telescope: From inception to realisation. Current Science 117:365–381, 1905.12896

Sánchez SF, Thiele U, Aceituno J, Cristobal D, Perea J, Alves J (2008) The Night Sky at the Calar Alto Observatory II: The Sky at the Near-infrared. Publications of the Astronomical Society of the Pacific 120(873):1244, DOI 10.1086/593981, 0809.4988

Singh R, Rastogi S (2018) Vibrational dynamics of phenylphenanthrenes with phenyl group at different positions. International Journal of Scientific Research in Physics and Applied Sciences 6:92–104, DOI https://doi.org/10.26438/ijcse/v6i5.92104, URL https://www.isroset.org/journal/IJSRPAS/full_paper_view.php?paper_id=902

Smith ECD, McLean IS (2008) A survey of 3.3 μm PAH emission in planetary nebulae. The Astrophysical Journal 676(1):408–415, DOI 10.1086/527370, URL https://doi.org/10.1086%2F527370

Stetson PB (1992) More Experiments with DAOPHOT II and WF/PC Images, Astronomical Society of the Pacific Conference Series, vol 25, p 297

Tielens A (2008) Interstellar Polycyclic Aromatic Hydrocarbon Molecules. Annual Review of Astronomy and Astrophysics 46(1):289–337, DOI 10.1146/annurev.astro.46.060407.145211, URL https://doi.org/10.1146/annurev.astro.46.060407.145211

Van de Sande M, Sundqvist JO, Millar TJ, Keller D, Decin L (2019) The chemistry in clumpy AGB outflows. In: Kerschbaum F, Groenewegen M, Olofsson

H (eds) IAU Symposium, IAU Symposium, vol 343, pp 531–532, DOI 10.1017/S1743921318005434

Van Winckel H (2003) Post-AGB Stars. Annual Review of Astronomy and Astrophysics 41(1):391–427, DOI 10.1146/annurev.astro.41.071601.170018, URL https://doi.org/10.1146/annurev.astro.41.071601.170018

Werner MW, Sahai R, Davis J, Livingston J, Lykou F, DE Buizer J, Morris MR, Keller L, Adams J, Gull G, Henderson C, Herter T, Schoenwald J (2014) Mid-infrared Imaging of the Bipolar Planetary Nebula M2-9 from SOFIA. The Astrophysical Journal 780:156, DOI 10.1088/0004-637X/780/2/156, 1311.4949

Woodward CE, Pipher JL, Shure M, Forrest WJ, Sellgren K (1989) Spectroscopic Images of NGC 7027 in the Near-Infrared Dust Emission Features. The Astrophysical Journal 342:860, DOI 10.1086/167642

Zijlstra AA, Loup C, Waters LBFM, de Jong T (1992) Interrupted mass loss on the asymptotic giant branch. Astronomy & Astrophysics 265:L5–L8

Ziurys LM (2006) The chemistry in circumstellar envelopes of evolved stars: Following the origin of the elements to the origin of life. Proceedings of the National Academy of Sciences 103(33):12274–12279, DOI 10.1073/pnas.0602277103, URL https://www.pnas.org/content/103/33/12274, https://www.pnas.org/content/103/33/12274.full.pdf

Zuckerman B, Gatley I (1988) Molecular hydrogen maps of extended planetary nebulae - The Dumbbell, the Ring, and NGC 2346. The Astrophysical Journal 324:501–515, DOI 10.1086/165910



Figure 1: The TIRCAM2 mounted at the main axial port of the 3.6 m DOT.

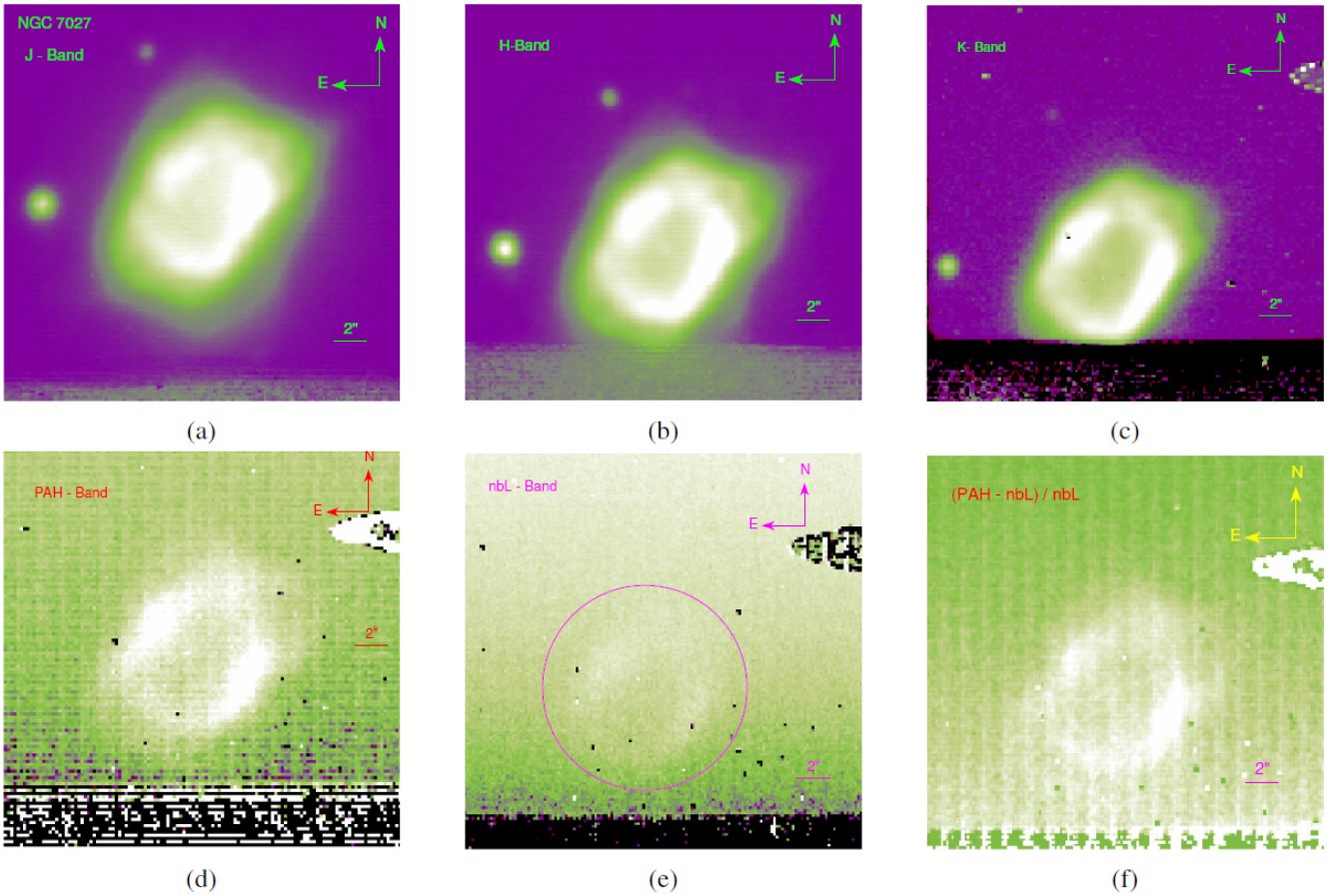


Figure 2: High-resolution images of NGC 7027 taken with TIRCAM2 on 3.6m DOT: (a) J, 1.2 μm; (b) H, 1.65 μm (c) K, 2.19 μm; (d) PAH, 3.28 μm; (e) nbL, 3.59 μm; (f) normalized continuum difference image, $(I_{PAH} - I_{nbL})/I_{nbL}$.

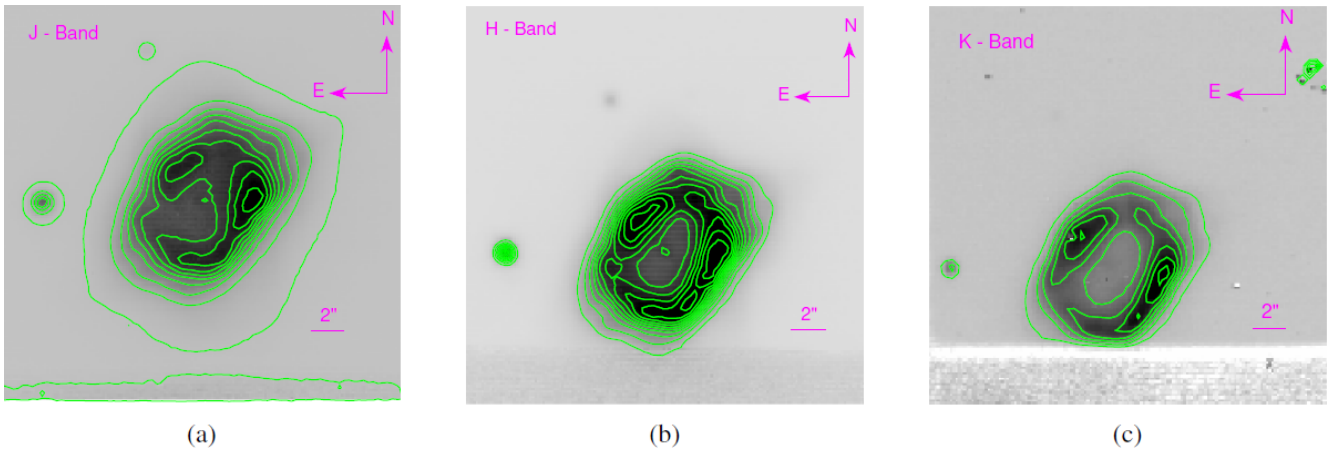


Figure 3: Contour images of NGC 7027 at: (a) J, 1.2 μm; (b) H, 1.65 μm; (c) K, 2.19 μm. Contours are separated by (a) 10%, (b) 7.3% and (c) 4% of corresponding peak values.

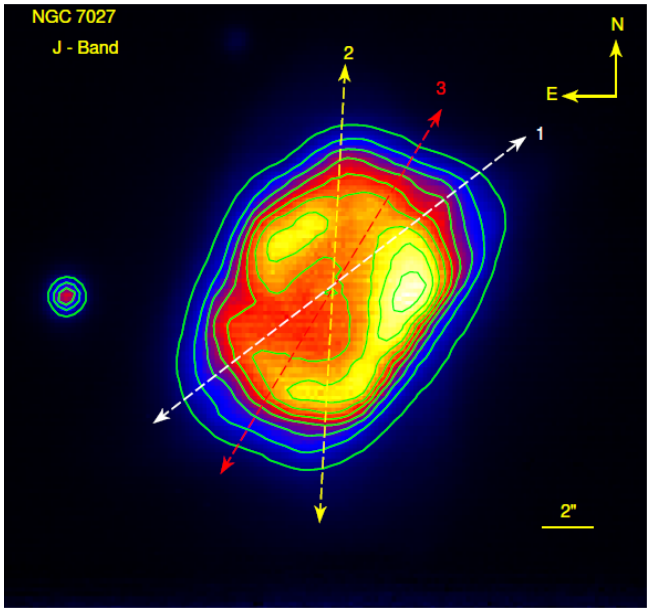


Figure 4: False color image of contour plot of NGC 7027 in J-Band with 1,2 and 3 outflow directions. The bi-directional arrows labelled 1-3 correspond to the direction of the outflows identified by Cox et al. (2002). Outflow 1 (white) is believed to be the most recent and/or powerful outflow.

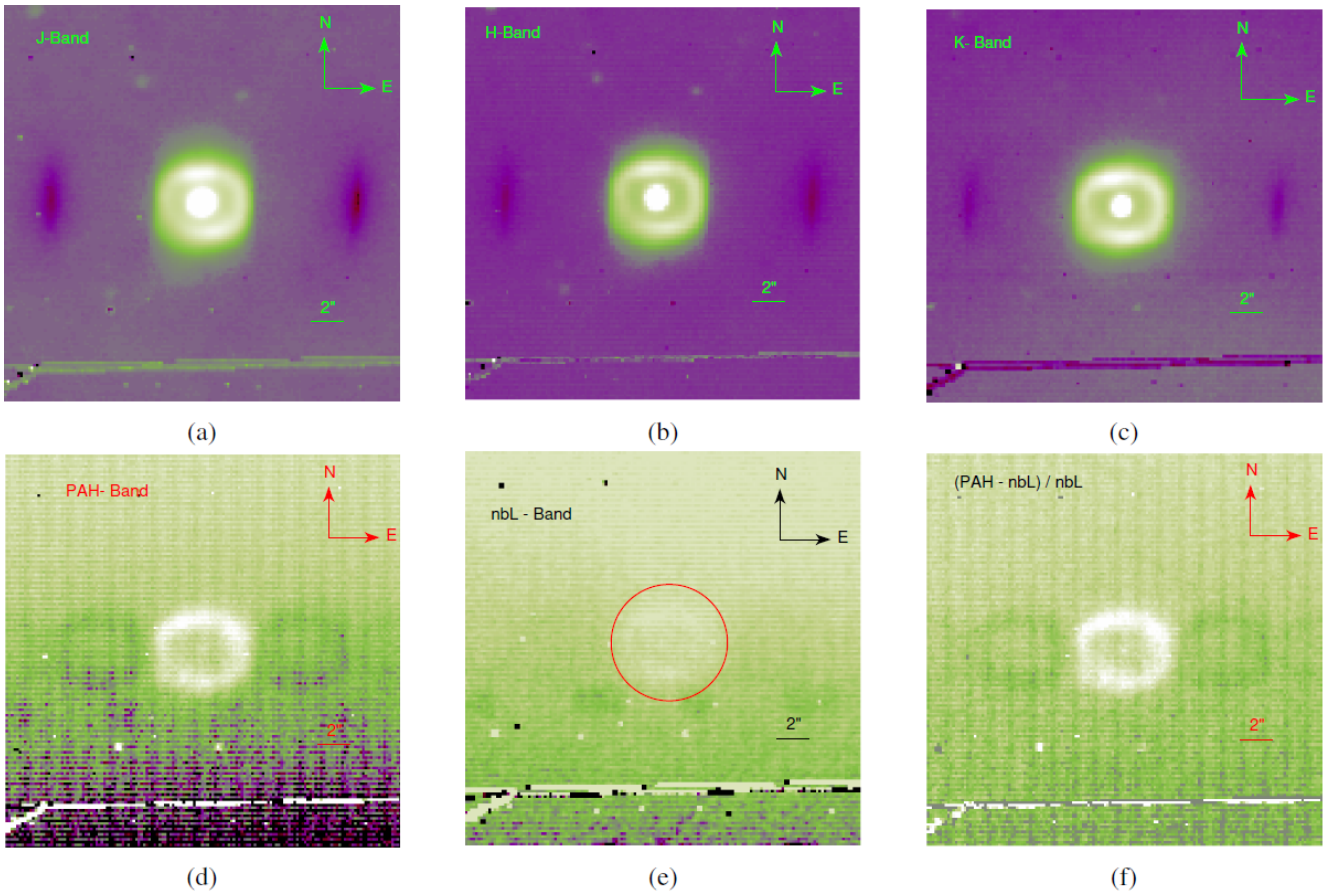


Figure 5: High-resolution images of BD +30° 3639 taken with TIRCAM2 on 3.6m DOT: (a) J, 1.2 μm; (b) H, 1.65 μm (c) K, 2.19 μm; (d) PAH, 3.28 μm; (e) nbL, 3.59 μm; (f) normalized continuum difference image, $(I_{PAH} - I_{nbL})/I_{nbL}$.

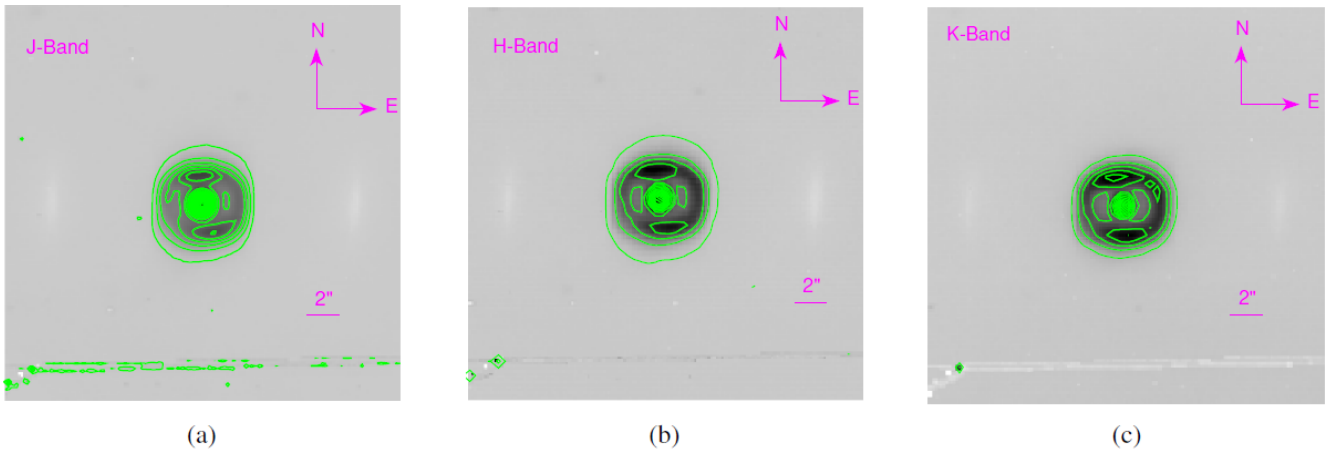


Figure 6: Contour images of BD +30° 3639 at: (a) J, 1.2 μm; (b) H, 1.65 μm (c) K, 2.19 μm. Contours are separated by (a) 3.5%, (b) 5% and (c) 6% of corresponding peak values.

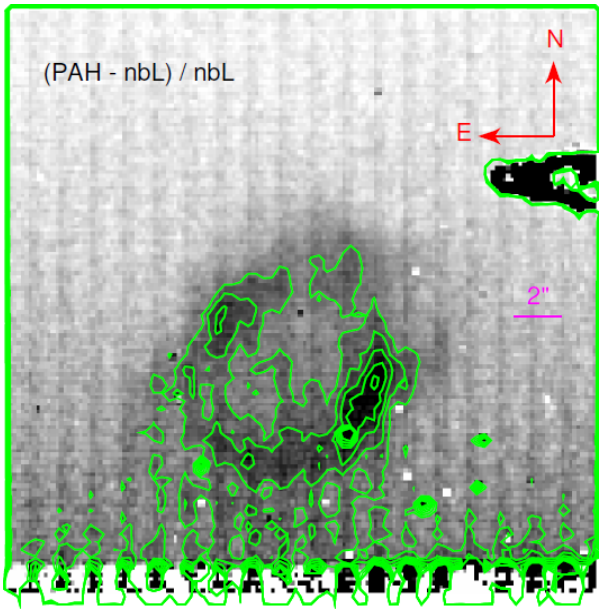


Figure 7: Contour image of NGC 7027 at 3.28μm. Contours are overlaid for clarity and are separated by 15% of peak value.

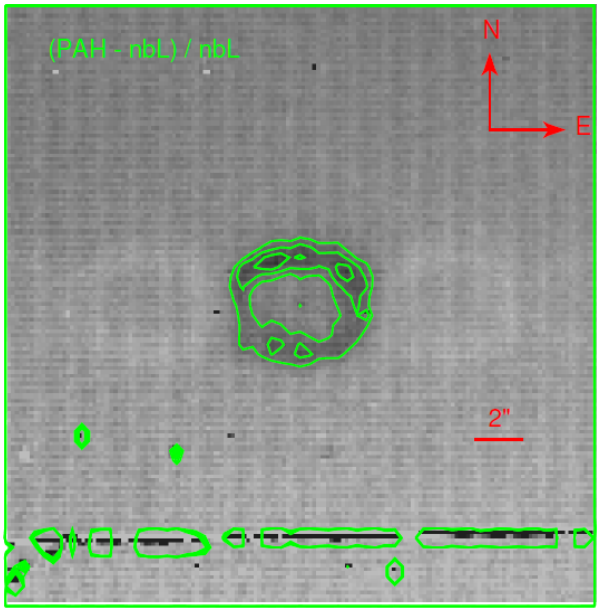


Figure 8: Contour image of BD +30° 3639 at 3.28μm. Contours are overlaid for clarity and are separated by 16% of peak value.

Table 1: TIRCAM2 Observation Details

Object Name	Filter	Dither Position	No. of frames	Exposure Time (sec)	Total Time Integration (sec)
NGC 7027	J	3	4	20	3 x 4 x 20 = 240
	H	3	4	20	3 x 4 x 20 = 240
	K	3	7	12	3 x 7 x 12 = 252
	PAH	3	300	0.05	3 x 300 x 0.05 = 45
	nbL	3	300	0.05	3 x 300 x 0.05 = 45
BD +30° 3639	J	3	3	8	3 x 3 x 8 = 72
	H	3	3	8	3 x 3 x 8 = 72
	K	3	5	5	3 x 5 x 5 = 75
	PAH	3	300	0.05	3 x 300 x 0.05 = 45
	nbL	3	300	0.05	3 x 300 x 0.05 = 45

Table 2: JHK Photometry of NGC 7027 and BD +30° 3639

Objects	**Standard Object***	**Filter**	**Aperture Radius** (arcsec)	**Magnitude**	**Mag. Error**
NGC 7027	FS04 (TYC 30-78-1)	J	10.55	6.86	0.003
		H	8.44	6.77	0.004
		K**	-	-	-
BD +30° 3639	FS25 (TYC 351-60-1)	J	4.14	9.72	0.005
		H	4.23	9.44	0.012
		K	3.43	8.21	0.009

* Hunt et al. (1998)
** magnitude could not be obtained as a large part of the K-band image overlaps bad patches in the lower side of the array.

Table 3: Size of NGC 7027

Filter	Angular diameter	Elliptical radius		Distance between central star and inner edge of the shell					Extended asymmetric region from center
		Semi major axis	Semi minor axis	NE-Direction	NW-Direction	SE- Direction	SW-Direction	Average distance	
	(arcsec)	(arcsec)	(arcsec)	(arcsec)	(arcsec)	(arcsec)	(arcsec)	(arcsec)	(arcsec)
J	14.03	6.76	4.12	1.69	2.84	2.80	2.61	2.49	~ 8.2
H	13.92	6.75	4.57	1.71	2.89	2.79	2.06	2.36	~8.2
K	12.83	6.75	4.57	1.51	3.12	3.09	2.27	2.49	~8.0
$AIB_{3.28}$*	14.03	7.14	5.19	1.79	3.05	2.81	3.11	2.69	~ 7.5
nbL	14.03	7.14	5.19	1.79	3.05	2.18	3.11	2.69	~ 7.5

* $AIB_{3.28} = (I_{PAH} - I_{nbL})/I_{nbL}$

Table 4: Size of BD +30° 3639

Filter	Angular Diameter (arcsec)	Angular size of central object (arcsec)	Distance between central star and inner edge of the shell			Ratio of pixel values of the central star & nebula	Thickness of ring-shaped emission (arcsec)
			N-S Direction	E-W Direction	Average distance		
J	8.28	2.20	0″.41	0″.82	0″.62	4.19	1.32
H	8.45	2.10	0″.40	1″.06	0″.73	4.17	1.33
K	6.86	1.98	0″.34	0″.83	0″.59	1.74	1.36
$AIB_{3.28}$*	6.93	-	1″.29	1″.70	1″.50	-	1.42
nbL	6.93	-	1″.29	1″.70	1″.50	-	1.42

* $AIB_{3.28} = (I_{PAH} - I_{nbL})/I_{nbL}$

Table 5: Basic data of NGC 7027 and BD +30°3639

Properties	NGC 7027	BD +30°3639
Temperature	200000 K [a]	47000 K [d]
Mass	3 - 4 $M_\odot$ [b]	< 3 $M_\odot$ [e]
Distance	880 ± 150 pc [c]	1520 ± 210 pc [f]
Age of the Nebula	600 years [c]	600-800 years [g]
Shell expansion velocity	17 Km/s [c]	22∓4 Km/s [h]
Nebula temperature	14500 K [c]	8500 K [e]
Electron density	$7x10^4$ cm^3 [c]	$11x10^3 cm^3$ [e]
C/O	1.46 [b]	1.1 [i]
Average location of $AIB_{3.28}$ emission from the central star	6170 AU	5270 AU

NGC 7027: [a]Latter et al. (2000), [b]Bernard Salas et al. (2000), [c]Masson (1989)
BD +30°3639: [d]Leuenhagen et al. (1996), [e]Bernard-Salas et al. (2003), [f]Akras and Steffen (2012), [g]Li et al. (2002), [h]Mellema (2004), [i]Aller and Hyung (1995)